PROCEEDINGS OF THE ROYAL SOCIETY A

rspa.royalsocietypublishing.org

Research

Article submitted to journal

Subject Areas:
Boundary layer theory, Flow separation, Perturbation analysis

Keywords:
Bluff-body flows, Interactive boundary layers, Massive separation, Rayleigh stage, Triple deck, Turbulence

Author for correspondence:
Bernhard Scheichl
e-mail: b.scheichl@tuwien.ac.at

Royal Society Publishing
Informing the science of the future

Gross separation approaching a blunt trailing edge as the turbulence intensity increases

B. Scheichl[1,2]

[1] Institute of Fluid Mechanics and Heat Transfer, Vienna University of Technology, Resselgasse 3/E322, 1040 Vienna, Austria

[2] AC²T research GmbH (Austrian Center of Competence for Tribology), Viktor-Kaplan-Straße 2C, 2700 Wiener Neustadt, Lower Austria

A novel rational description of incompressible two-dimensional time-mean turbulent boundary layer flow separating from a bluff body at an arbitrarily large globally formed Reynolds number, Re, is devised. Partly in contrast to and partly complementing previous approaches, it predicts a pronounced delay of massive separation as the turbulence intensity level increases. This is bounded from above by a weakly decaying Re-dependent gauge function (hence the boundary layer approximation stays intact locally) and thus the finite level characterising fully developed turbulence. However, it by far exceeds the moderate level found in a preceding study which copes with the associated moderate delay of separation. Thus, the present analysis bridges this self-consistent and another forerunner theory, proposing extremely retarded separation by anticipating a fully attached external potential flow. Specifically, it is shown upon formulation of a respective distinguished limit at which rate the separation point and the attached-flow trailing edge collapse as $Re \to \infty$ and how on a short streamwise scale the typical small velocity deficit in the core region of the incident boundary layer evolves to a large one. Hence, at its base the separating velocity profile varies generically with the one-third power of the wall distance, and the classical triple-deck problem describing local viscous/inviscid interaction crucial for moderately retarded separation is superseded by a Rayleigh problem, governing separation of that core layer. Its targeted solution proves vital for understanding the separation process more close to the wall. Most important, the analysis does not resort to any specific turbulence closure. A first comparison with the available experimentally found positions of separation for the canonical flow past a circular cylinder is encouraging.

1. Motivation and introduction

Let us consider incompressible, isoviscous cross-flow around a (closed) rigid, blunt obstacle at rest in the frame of reference with a smooth impervious cylindrical surface aligned with the spanwise flow direction in an otherwise unbounded domain. Let the Reynolds number Re formed with the speed $\tilde{U}$ of the undisturbed uniform flow infinitely far upstream of the body, a characteristic value $\tilde{R}$ of the radius of its surface curvature, and the (constant) kinematic viscosity, take on arbitrarily large values. We are then concerned with the formation of a nominally steady and two-dimensional turbulent boundary layer (BL) along the body surface, which finally undergoes gross (i.e. massive, developed, or break-away) separation. We furthermore disregard any effects of free-stream turbulence, surface tension at play along the two dividing streamlines separating the free-stream region and that of rather weakly recirculating flow, and body forces as gravity. By ignoring the complex picture of the flow in the region representative for the obstacle dimensions and the wake emerging further downstream, our concern is with a (most) rigorous description of the local separation process, in particular the prediction of its location, by exploiting the time- or Reynolds-averaged Navier–Stokes or Reynolds equations for $Re \to \infty$. Insofar and like in the preceding studies surveyed next, an *ab initio* theory is the ultimate goal of the efforts: turbulence modelling is only invoked when it comes to quantitative predictions as the asymptotic properties of the flow are universal.

Notwithstanding the undeniable progress made in the last decades by rigorous application of perturbation methods, its completion still poses one of the most challenging problems in theoretical hydrodynamics. As achieving seminal progress towards its solution, the outstanding study [1] must be viewed as a milestone: it was not until its advent that the regularisation of the inevitable Brillouin–Villat (B–V) singularity forming at detachment of the external potential flow, which then encloses a dead-water cavity further downstream, was addressed correctly within the framework of triple-deck theory. Here, the well-established picture of strictly laminar (steady) flow served as a starting point, where we refer to the textbook [2] and the corresponding references therein for a seminal overview. However, the first attempt to deal with turbulent gross separation must be attributed to the asymptotic treatment [3] of the turbulent flow past an inclined flat plate as the external potential admits a singularity of B–V type at the trailing edge. Most important, in contrast to the laminar-flow situation, cf. [2], in this typical setting (forming the starting point for advanced studies of the practically important class of flows around thin-airfoil of more general shape) the angle of attack may be even of $O(1)$. This finding merely relies on the assumption of a fully developed turbulent BL but the actual mechanism of separation, i.e. the flow in the viscous wall layer and the near-wake, could be largely ignored. (Unfortunately, the analysis is then also not capable of assessing the violation of the Kutta condition by viscous effects in turbulent trailing-edge flow.) The series of papers [4–6] represents a definite leap forward in the description of separation from a bluff body insofar as the regularisation of the pronounced B–V singularity at play is taken into account in a self-consistent manner. One has to concede, however, that the proposed theory is a purely local one, and no attempt was made to embed the local structure of the flow into a global setting at length scales comparable to the characteristic body dimensions. Also, and as pointed out first in [7], the proposed three-tiered structure of the BL implies a mismatch in the overlap of its main and the viscous wall layer. This inherently occurs because the relative streamwise velocity deficit in the former flow region is of $O(1)$ rather than measured by the principal perturbation parameter $\epsilon := \kappa/\ln Re$, with κ denoting the von Kármán constant, as it is the case in the well-established classical two-tiered picture of a turbulent BL. There the slenderness of the BL scales with ϵ too. The large velocity defect is nevertheless deemed required in the light of the mechanisms governing laminar-flow separation. This idea was taken up in the latter study [7], but there the description of the BL flow is accomplished through the introduction of a slenderness parameter independent of Re. Here realistic values for this quantity are determined on an empirical basis or extracted from the small constants appearing in algebraic but also more sophisticated turbulence models when these are

examined within the framework of the associated formal two-parameter asymptotic analysis. The wall slip arising at the base of the resulting wake-type velocity profile in the outer main part of the again three-tiered BL was considered to resolve the deficiencies of the previous approaches. However, matching the velocity profiles in the intermediate and the innermost viscous wall layer once more proves inconsistent with that *a priorly* stipulated *Re*-independence.

A yet seriously weaker reasoning in the theory put forward in [7] — as apparently unrecoverable in an attempt to amend and complete it — is given by the absence of the B–V singularity in the external flow as its regularity intrinsically inhibits massive separation of the BL. The latter discrepancy bears resemblance to that encountered in the fundamental study [8] on extending laminar BL flow through a point of vanishing skin friction indicating the onset of gross separation. This finally supports the necessity to seek the external potential flow in the class of free-streamline or Kirchhoff flows.

Eventually, the theory presented in [1] and refined in [9] masters all the shortcomings arising in the forerunner studies. At first, it adopts the classical two-tiered structure of the incident turbulent BL to the extent as it exhibits the well-known asymptotically small velocity defect in its main tier. Simultaneously, however, the BL thickness is reduced in its order of magnitude when compared to that of a fully developed turbulent BL, due to the process of laminar–turbulent transition shortly downstream of the front stagnation point or leading edge of the obstacle as demonstrated [10]. This embedding of the BL into a global flow picture implies that the actual BL represents a member of the family of *slightly underdeveloped* turbulent BLs parametrised by the novel (here redefined) gauge factor $T \lesssim 1$ which measures the relative level of the turbulence intensity or, in other words, the ratio between the slenderness and the relative velocity deficit of $O(\epsilon)$. The limits $T = 1$ refer to the classical flow picture and the situation of a perfectly laminar BL. Next, the effective dependence of T on *Re* and hence the scaling of the BL follows from the interaction mechanism governing the separation process. As shown in [9], this mechanism is twofold: an internal triple-deck structure with the viscous wall layer serving as the main deck is embedded in a Euler stage evolving from the local breakdown of the oncoming small-deficit main layer and accounting for weak perturbations about the local state of the flow therein. A linear vortex-flow problem is the central ingredient of the Euler region, as in [3]. However, the local flow structures differ distinctly in detail as a consequence of the reduced turbulence intensity level in [9]. Therefore, the neglect of explicit viscous effects in [3] renders this analysis of trailing-edge flows incomplete if not questionable at all. Furthermore, in [9] the strength of the B–V singularity is measured by the so-called B–V parameter $k\,(>0)$, which increases monotonically for increasing distances between leading-edge stagnation and separation (relative to the typical body dimension $\tilde{R}$): see also [9–12]. We recall that gross separation of purely laminar flow applies if $k = O(Re^{-1/16})$ [2] but a considerable level of turbulence intensity in the BL requires $k = O(1)$. Formally, k takes the place of the inclination angle in [3], but in the present setting of self-induced separation its effective value remains arbitrary as long as it refers to semi-open cavities embedded in the Kirchhoff flows [9].

In other words, the existing theory of turbulent separation is indeed self-consistent both locally and globally but has proven incomplete in the latter sense. To be more specific, the required match of the solution of the upper-deck equations, describing the internally induced potential flow, and that of the vortex-flow problem, at play on the BL scale, does not yield a constraint fixing the value of k, in contrast to original expectations.

Specifically, the viscous-inviscid interaction described by the triple deck and regularising the B–V singularity in the near-wall regions of the BL results the an appealingly concise relationship

$$T \propto \left[k^{8/9}/u_d(k)^{4/9}\right] Re^{-4/9}/\epsilon^2 \quad \text{for} \quad k = O(1)\,. \tag{1.1}$$

Herein u_d denotes the flow speed due to the Kirchhoff flow at detachment, made non-dimensional with $\tilde{U}$, and the omitted proportionality constant of $O(1)$ is part of the triple-deck solution; see [1,9] and the study [13] on the non-interactive flow. Thorough parametric (numerical) studies of the class of Kirchhoff flows, see e.g. [12], indicate that for a given circulation these

depend continuously and uniquely on the parameter k, where the semi-open stagnant-flow wake confined by the free streamlines closes when k exceeds a certain threshold. Its then finite streamwise extent shrinks monotonically when k increases further. Finally, when k increases above all bounds it reduces to a single point which then forms the trailing edge of the body. Hence, this singular limit points to a perfectly attached potential flow, obtained formally for $k=\infty$. Guided by this view, we condense the two central shortcomings of the available theory into the following statements:

(i) neither the correct value of k could be determined so far under the premise that $k=O(1)$,
(ii) nor a self-consistent flow picture could be completed in the specific limit $k=\infty$, $T=1$ as $Re\to\infty$ anticipated in [1], i.e. with fully developed turbulence found to be tied in with a fully attached potential flow.

More precisely, considering the inviscid local self-interaction of the BL governed by a vortex-flow problem, neglected in [1] in the case addressed in (ii), in the follow-up analysis in [11] led to an inconsistency. This renders the theory in [1] not full-fledged. Consequently, settling the question

How do k and T vary with Re in a distinguished limit $Re\to\infty$, $k\to\infty$ yet to be suitably defined?

is crucial for completing the theory of gross separation as described by these three asymptotic key parameters. Specifically, the formulation of the extreme flow case mentioned in (ii) demands a critical revision and refinement. We hence commence the analysis by scrutinising the external flow for large values of k before we establish the distinguished limit and focus on the consequences.

2. Kirchhoff flow with infinitesimally small cavity

For what follows, we tacitly refer to the configuration sketched in Figure 1*(a)*.

For the sake of simplicity, the body and, consequently, the flow are assumed to have an axis of symmetry aligned with the unperturbed flow. Hence, the flow is free of circulation. The value of the B–V parameter k shall be so large that the cavity emerging in the inviscid-flow limit and exhibiting fluid at rest is closed. Let the natural coordinates s, n pointing along and normal from the contour of the body, respectively, and having their origin in its leading edge (front stagnation or branching point of the flow) be non-dimensional with $\tilde{R}$, the velocity components u, v in the streamwise and normal directions, respectively, with $\tilde{U}$, and the local pressure difference p with respect to flow stagnation as well as the components r_{ij} (i, j stand for s, n) of the Reynolds stress tensor with the dynamic head formed with $\tilde{U}$. We furthermore introduce a streamfunction ψ such that $u=\partial\psi/\partial n$. The Kirchhoff flow is obtained in the inviscid limit $[u,v,p]\sim[u^0,v^0,p^0](s,n;k)$ as $Re\to\infty$, such that $u_s(s;k):=u^0(s,0;k)$ denotes the surface speed it exerts on the body surface. The B–V singularity occurs immediately upstream of the position of inviscid-flow detachment, $s=s_d(k)$, with $\mathrm{d}s_d/\mathrm{d}k>0$. We give the classical result [2,9,14] for

$$h:=s-s_d\to 0_+:\quad u_s(s;k)/u_d(k)\sim g(h)+O\big(h^{3/2}\big)\,,\quad g(h):=1+2\sqrt{h}+10\,h/3\,. \tag{2.1}$$

Here the remainder terms are affected by the local surface curvature but the subsequent analysis is not. We now have $u_d(k)=u_s(s_d,k)$, equal to the flow speed on the free streamlines downstream of detachment.

The aforementioned modification of the Kirchhoff flow towards a fully attached flow is completed in the limit $k=\infty$ where the two detachment points, the one considered given by $(s,n)=(s_d,0)$, have merged at the thus arising trailing edge (rear stagnation point), $(s,n)=(s_t,0)$ with $s_t:=s_d(\infty)$. Hence, this adjustment for $k\to\infty$ deserves to be elucidated from an asymptotic viewpoint. One conveniently considers this limiting behaviour by letting the distance $d(k):=s_t-s_d(k)$ become arbitrarily small. At the body scale, we then write $[u^0,v^0](s,n;k)\sim[u^0,v^0](s,n;\infty)+O(d^4)$. In turn, we have $[u^0,v^0](s,n;\infty)\sim\lambda\sigma+O(\sigma^3)$ as $\sigma:=s_t-s\to 0_+$, with the constant $\lambda\,(>0)$ depending on the overall body shape. In these expansions the remainder terms stem from matching with the flow in the emerging subregion of streamwise and lateral extent d that encompasses the detachment and stagnation points and

the accordingly shrunken cuspidal cavity. We note the well-known results

$$u_s(s;\infty) = 2\sin s\,, \quad s_t = \pi\,, \quad \lambda = 2 \tag{2.2}$$

referring to the important canonical case of attached flow about a circular cylinder (unit circle).

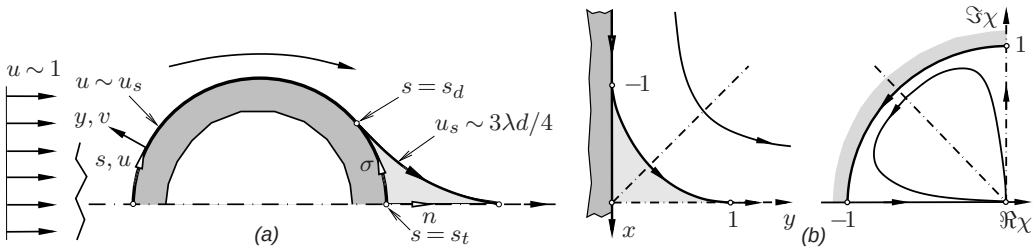

Figure 1. Flow configuration *(a)*, conformal mapping $z \mapsto \chi$ *(b)*: cavity in the Kirchhoff-flow limit *light-shaded*

The stretched (locally Cartesian) variables $(x, y) := (-\sigma, n)/d$ are appropriate for that subregion, locally symmetric with respect to $x = 0$ and $y = -x$. In that region we have the inner expansions $[u, v] \sim \lambda d\,[\bar{u}, \bar{v}](x, y)$, $p \sim (\lambda d)^2 \bar{p}(x, y)$ and conveniently describe the leading-order potential flow in terms of the complex potential $\bar{w}(z)$, $z := x + \mathrm{i}y$, with $\bar{w}'(z) = \bar{u} - \mathrm{i}\bar{v}$. It can be expressed analytically by virtue of a conformal mapping of the flow region in the physical complex z-plane for $x < 0$ onto the interior of the upper quarter-unit circle in an auxiliary χ-plane, see Figure 1*(b)*: the origin $\chi = 0$, the boundary of that quarter-circle, and the branching points $\chi = -1$ and $\chi = \mathrm{i}$ of $\bar{w}$ are the images of $z = \infty$, the free streamline (separatrix) confining the stagnant-flow cusp, its point $z = \mathrm{i}$ of merging with its counterpart stemming from the flow along the surface for $x > 0$ or $s > s_t$, and the location of flow detachment, $z = -1$, respectively. On the separatrix the kinematic and dynamic boundary conditions, respectively, $\Im\bar{w}(z) = 0$ and $|\bar{w}'(z)|$ equal to the initially unknown flow speed $\bar{u}_d := \bar{u}(-1, 0)$ at detachment hold. One then readily uses the representations $\bar{w}(z) = (\bar{u}_d^2/2)(\chi + 1/\chi)^2$, $\bar{w}'(z) = \mathrm{i}\bar{u}_d/\chi$. Elimination of χ confirms the match with the outer stagnating flow as $\bar{w} \sim -z^2/2$ for $(x, y) \to (-\infty, \infty)$. Finally, subsequent integration gives for the entire flow region in the upper half of the z-plane

$$-z = (-\breve{w})^{3/2} + (1 - \breve{w})^{3/2}\,, \quad \breve{w} := 8\bar{w}/9\,, \quad \bar{u}_d = 3/4\,. \tag{2.3}$$

The above mapping onto the two branching points provides a constraint expressed by the last result, hereafter tacitly invoked when $\bar{u}_d$ is used. We note the branch cuts in the $\breve{w}$-plane along the images $1 < \breve{w}$ and $0 < \breve{w} < 1$ of the merged streamlines and the separatrix, respectively. The latter is represented by a quarter of the tetracuspid (asteroid) $x^{2/3} + y^{2/3} = 1$ $(-1 < x < 0,\, 0 < y < 1)$.

The B–V singularity is revealed in the form $\bar{w}'(z)/\bar{u}_d \sim 1 + \mathrm{i}\sqrt{(z+1)/6} + O(z+1)$ as $z \to -1$. As the gauge pressure $\bar{p}(z) - \bar{p}(-1)$ is given by Bernoulli's law or $\bar{u}_d^2/2 - |\bar{w}'(z)|^2/2$, we find for

$$z \to -1: \quad \bar{p}(z) - \bar{p}(-1) \sim -2\bar{u}_d^2\,\Im\sqrt{(z+1)/6} + O(z+1)\,. \tag{2.4}$$

Specifically, with $\bar{u}_s(x) := \bar{w}'(x)$, $x \le -1$, being the surface slip exerted by the leading-order inner solution, one extracts from the implicit representation (2.3) for $\bar{w}(z)$ an inverse one for $\bar{u}_s(x)$,

$$-x(\bar{u}_s) = \bar{u}_s + (\bar{u}_d/\bar{u}_s)^3/4 \quad (x \le -1)\,. \tag{2.5}$$

This gives rise to the expansions for

$$x \to -\infty: \quad \bar{u}_s \sim -x + O(x^{-3})\,, \quad S := -1 - x \to 0_+: \quad \bar{u}_s/\bar{u}_d \sim g(S/6) + O\big(S^{3/2}\big)\,, \tag{2.6a,b}$$

with g taken from (2.1). In Figure 2*(a)* $\bar{u}_s$ is plotted versus x together with the asymptotes given explicitly by (2.6). The behaviours (2.6a) and $u_s(x;k)/d \sim \bar{u}_s(x) + O(d)$ agree by matching. Most

important, (2.6b) recovers the universal part of the B–V singularity in the form (2.1) provided the following important leading-order estimates hold for

$$d \to 0: \quad k \sim 1/\sqrt{6d}\,, \quad u_d \sim 3\lambda d/4\,. \tag{2.7}$$

This dependence of d on k completes our analysis of the limiting state of Kirchhoff flows.

Two side issues are noteworthy: At first, the inner leading-order solution (2.3) can also be extracted from well-known Kolscher's solution [15] describing the family of flows past a splitter plate. Secondly, it can be generalised in a physically viable manner (from the viewpoint of the high-*Re*-limit). To this end, we only consider the region $x \geq 0$ and substitute z by $[z^{2\alpha} + H(1/2-\alpha)]^{1/2}$ with some $\alpha > 0$ and H denoting the Heaviside step function. Then (2.3) recovers the patterns of potential flows around an internal stagnation zone adjacent to a kinked wall formed by the ray $\arg z = \pi/(2\alpha)$ and the positive x-axis: for $1/4 < \alpha < 1/2$ it is convex towards the flow and the cavity located along the ray immediately downstream of $z = 0$; for $1/2 < \alpha < \infty$ it is concave and the flow symmetric with respect to the line $\arg z = \pi/(4\alpha)$; for $\alpha = 1/2$ the flow represents a special member of the Batchelor–Sadovskii potential-vortex flows. Flows parametrised by α were calculated first in [16] by a more elaborate conformal-mapping technique.

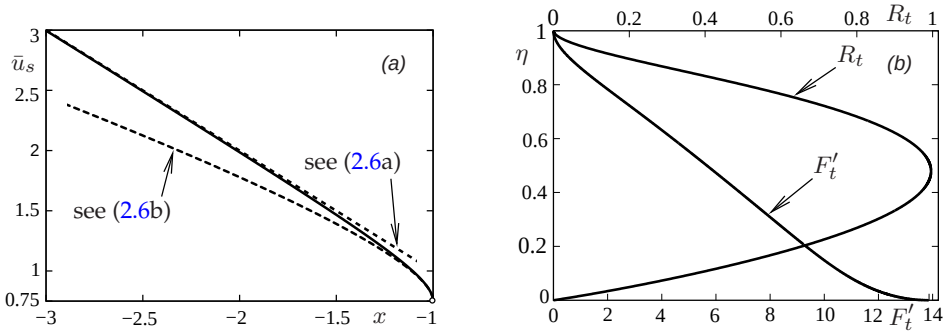

Figure 2. Surface slip (*solid*) by (2.5) with asymptotes (*dashed*) *(a)*; universal BL profiles near stagnation by (3.4) according to [17], copyright transfer by Springer Publishing is greatly acknowledged *(b)*

3. Incident boundary layer

We next consider the slightly underdeveloped oncoming two-tiered turbulent BL when approaching the inner Chaplygin-flow square region of extent d. We will only focus on the behaviour of the core layer. This will first extend the existing theory as available by [9] towards the limit $k \to \infty$.

(a) Splitting of small-defect flow revisited

According to [9], in a sublayer of wall-normal extent δ_l, say, the Reynolds stresses r_{ij} scale with $(\delta_l\, \partial_u/\partial_n)^2$. Hereafter partial derivatives are indicated by subscripts unless this may cause confusion. For $0 < s < s_d$ thus the inner expansion

$$\left\{\left[\frac{u_s n - \psi}{u_s \epsilon \delta}, \frac{r_{ij}}{u_s^2 \epsilon^2 T}\right], \frac{\delta}{\epsilon T}\right\} \sim \left\{[F_\eta, R_{ij}](s,\eta;k),\, \Delta(s;k)\right\} + O(\epsilon)\,, \quad \eta := \frac{n}{\delta} = O(1)\,, \tag{3.1}$$

describes the core layer exhibiting a velocity defect of $O(\epsilon)$. Here δ denotes the thickness of the BL having a rather abrupt outer edge (the disregard of a thin overlayer on top of the core layer does not affect the present analysis), and the streamfunction F as well as the shape functions $R := R_{sn}$,

Δ of the Reynolds shear stress and the BL edge are governed by the leading-order BL problem

$$\frac{\mathrm{d}(u_s\Delta)}{\mathrm{d}s}\frac{\eta F_\eta}{u_s}-\frac{1}{u_s^3}\frac{\partial(u_s^3F\Delta)}{\partial s}=R-1\,,\quad \eta\to 0:\ \ F\to 0\,,\ \ R\to 1\,,\quad \eta=1:\ \ F_\eta=R=0\,, \tag{3.2}$$

subject to initial conditions reflecting the match with the transitional flow as $s\to 0$, and to be supplemented with a suitable closure for R. The match with the viscous wall layer for $\eta\to 0$ is provided via that of the Reynolds and the wall shears stress, associated with the celebrated logarithmic law of the wall: $R\sim 1$, $F_\eta\sim-\kappa^{-1}\ln\eta+C(s;d)$; the intercept C is part of the solution of (3.2). The outer expansion of the potential flow, i.e. of u_s, as $k\to\infty$ triggers the regular corresponding one $[F,R,\Delta]\sim[F^\infty,R^\infty,\Delta^\infty](s,\eta)+O(d^4)$, again to be considered for $\sigma\to 0_+$.

As shown in [1,11], the least-degenerate behaviour of F_∞, R_∞, Δ_∞ in this limit means a rapid increase of the velocity deficit and the BL thickness. Specifically, examination of (3.2) yields for

$$\sigma\to 0_+:\ \ \left[F^\infty,\,R^\infty,\,\Delta^\infty\right]\sim\left[\frac{\sqrt{f}\,F_t(\eta)}{\sigma^2\sqrt{-\ln\sigma}},\,\frac{f\,R_t(\eta)}{\sigma^4(-\ln\sigma)},\,\frac{4\sqrt{-f\ln\sigma}}{\sigma F_t(1)}\right],\ \ f:=\int_0^{s_t}\frac{u_s^3(s;\infty)}{4\,\lambda^3}\,\mathrm{d}s\,. \tag{3.3}$$

Thus, the flow near the trailing edge is represented by the shape functions F_t and R_t of $O(1)$, and the factor f accounts for its upstream history. Inspection of the streamwise component of the Reynolds equations shows that the flow in the core layer becomes predominantly inviscid immediately upstream of stagnation. Measures $\sigma\epsilon F_\eta$ the velocity deficit as $u_s=O(\sigma)$, we have $r_{sn}=O(T\sigma^2\epsilon^2F_\eta^2)$. This result then follows from casting the assertion $u\,\partial u/\partial s\gg\partial r_{sn}/\partial y$ into the order-of-magnitude estimate $\sigma^2\epsilon F_\eta/\sigma\gg T(\sigma\epsilon F_\eta)^2/\delta$, which gives $\Delta^\infty/\sigma\gg F_\eta^\infty$, confirmed by (3.3). Accordingly, the left-hand side of the BL equation in (3.2) is satisfied identically to leading order. On account of the logarithmic variations of σ, (3.2) assumes the universal form

$$2\eta F_t'=F_t(1)\,R_t\,,\ \ F_t'(1)=R_t(1)=R_t(0)=0\,. \tag{3.4}$$

Since the behaviour (3.3) accompanies a splitting of the core layer, the leading-order stresses at the base of its main part and, in turn, the inhomogeneities in (3.2) vanish. Therefore, the logarithmic law of the wall still holds in the overlap between the new intermediate and the viscous wall layer but a reduced wall slip on its top due to a positive value of $F_t'(0)$ and a square-root behaviour now provides the match of the new core and the intermediate layer for

$$\eta\to 0:\quad F_t'\sim F_t'(0)-a\sqrt{\eta}\,[1+o(\eta)]\qquad a:=(2/\kappa)\sqrt{2F_t'(0)/F_t(1)}\,. \tag{3.5}$$

This terminal state of the BL was not taken into account in [1] but recognised first in [11].

Remarkably, such a tree-tiered flow structure associated with a moderately large velocity deficit (here given by the growth rate of F^∞ in (3.3) taking place at a streamwise extent $\sigma\ll 1$) is known to apply to turbulent BLs prone to mild separation. On condition of leading-order equilibrium, these are are also governed by (3.4), see [17]. Hence, we chose the prefactors in (3.3) so as to obtain (3.2) in this specific form and adopt the numerical solution to this problem put forward in [11]. It employs an asymptotically correct algebraic mixing-length model for R and is presented in Figure 2*(b)*. The near-wall behaviour (3.5) is clearly discerned. Our experience with other algebraic models is that they give numerically close results.

(b) Large-defect flow

The mechanism of breakdown of the BL limit, initiated by its above splitting, is twofold: it is due

(I) an increased relative velocity defect of $O(1)$ in the core layer so that the linearisation of the convective terms in the BL equation, see (3.2), ceases to be valid,

(II) or/and the emergence of a square region where $\sigma/\delta=O(1)$, giving rise to an Euler stage.

According to (3.3), a velocity deficit of $O(1)$ as considered in case (I) applies if σ is shortened and δ has increased to $O(\tau)$ and $O(\mu)$, respectively, with

$$\tau := (2^{5/4} f^{1/4}/3^{1/2})\, \epsilon^{1/2}/(-\ln \epsilon)^{1/4}\,, \quad \mu := 3\,\tau T(-\ln \epsilon)/[2F_t(1)]\,. \tag{3.6}$$

Making use of these quantities, we next consider case (II) given the small-defect assumption can be maintained: $\sigma/\tau \gg 1$. On condition that k is so large that $d \ll \sigma$ and the presence of the B–V singularity not perceptible on the considered length scale σ, this situation refers to case (ii), Section 1, and is therefore here discarded. For values of k just so large that $\sigma/d = O(1)$, i.e. $d/\tau \gg 1$, we arrive at the terminal extension of the theory put forward in [1,9]. Then (1.1) must be replaced by $T \propto \phi(d)\, d^{-8/9} (\lambda Re)^{-4/9} \epsilon^{-2}$ upon substitution of (2.7) and with the additional factor $\phi(d) := d^3(-\ln d)^{3/4}$ introduced to account for the increase of δ/ϵ^2 according to (3.3) (so that the $O(1)$-constant of proportionality now depends on the upstream history of the flow). However, this estimate still relies upon the concept of viscous-inviscid interaction, described by an internal triple-deck problem, and the linear response of the square core region, now exhibiting a moderately large velocity defect, on the B–V singularity. Hence, as seen from the above estimates and the definition of τ in (3.6), the ratio of δ and the thickness of the viscous wall layer and, in turn, T essentially still depend algebraically on Re. A desired drastic increase of the turbulence intensity is therefore not accomplished by this limit.

We are thus left with case (I). Reverting to the estimate given in Section 3(a), we now find that the inertia terms are larger than the wall-normal gradient of the Reynolds shear stress by a factor of $O(-\ln \tau)$ or $O(-\ln \epsilon)$. The formation of a fully nonlinear Euler stage (as indicated by "and" initiating case (I) above) is prevented in favour of its BL approximation, which accommodates a pronounced velocity defect. Hence, further analytical progress enabled, when we require that

$$\mu/\tau \ll 1 \quad \Leftrightarrow \quad T \ll -1/\ln \epsilon \sim 1/\ln\ln Re\,. \tag{3.7}$$

This finally represents a considerably weaker constraint for the turbulence intensity level than that given by (1.1). The interplay with the splitting of the Kirchhoff flow as $d \to 0$ is captured in terms of a least-degenerate distinguished limit governed by a similarity parameter, $D := d/\tau$, taken as of $O(1)$. The potential flow in the inner region considered in Section 2 then drives that BL.

Hence, x and $Y := n/\mu$ represent appropriate (locally Cartesian) BL coordinates of $O(1)$. We expand $\psi/\mu \sim \lambda\tau\hat{\Psi}(x, Y; D) + O(-\tau/\ln\tau)$, $\delta \sim \mu\hat{\Delta}(x; D) + O(-\mu/\ln\tau)$ where we note that $r_{sn} = O(Tu^2)$. Then the leading-order streamfunction $\hat{\Psi}$ satisfies Bernoulli's law,

$$\hat{U}(x, \hat{\Psi}; D) := \hat{\Psi}_Y = \sqrt{\bar{u}_{sD}(x)^2 + 2\hat{B}(\hat{\Psi})}\,, \quad \bar{u}_{sD} := D\bar{u}_s \quad \hat{B} := -3F_t'/4\,, \tag{3.8}$$

here expressed in von Mises variables. Here the specification of the Bernoulli function $\hat{B}$ follows from the match with the splitting small-defect flow upstream, where the factor $3/4$ (proving computationally advantageous subsequently) has its source in the choice of the proportionality constants in (3.6). Hence, $3F_t''(\hat{\Psi})/4$ represents the vorticity carried along the streamlines. The first relationship in (3.8) is valid for $0 \le \hat{\Psi} \le 1$ or $0 \le Y \le \hat{\Delta}$ and as long as

$$\bar{u}_s \ge \bar{u}_s^* := \sqrt{3F_t'(0)/(2D^2)} \quad \text{or} \quad x \le x^* := x(\bar{u}_s^*) \le -1\,, \tag{3.9}$$

see (2.5). For $x \le x^*$, the core layer exerts the slip $\hat{U}_s := \hat{U}(x, 0; D) = \sqrt{\bar{u}_{sD}(x)^2 - 3F_t'(0)/2}$ on the flow regions more close to the surface, and $\hat{\Psi}$ and the rescaled BL thickness $\hat{\Delta}$ are determined by

$$[Y,\, \hat{\Delta}(x; D)] = \left[\int_0^{\hat{\Psi}}, \int_0^1\right] \frac{\mathrm{d}\nu}{\hat{U}(x, \nu; D)}\,. \tag{3.10}$$

The BL structure is essentially characterised by $\bar{u}_{sD} \to +\infty$ far-upstream. Without resorting to a specific form of $\hat{B}(\hat{\Psi})$, one detects the generic small-deficit structure such a BL admits there: $\hat{U} \sim \bar{u}_{sD} + \bar{u}_{sD}^{-1}\hat{B}(\bar{u}_{sD}\hat{\Delta}\eta) + O(\bar{u}_{sD}^{-3})$ and $\hat{\Delta} \sim \bar{u}_{sD}^{-1} + O(\bar{u}_{sD}^{-3})$, with η, from here on redefined as $Y/\hat{\Delta}$, taken as of $O(1)$. Specifically, we have $\hat{\Delta} \sim \bar{u}_{sD}^{-1} + 3\bar{u}_{sD}^{-3}F_t(1)/4 + O(\bar{u}_{sD}^{-5})$ as $x \to -\infty$, and matching with the oncoming small-deficit BL is confirmed by virtue of (2.6a).

Let us first consider the two limiting cases

$$D \ll 1: \quad \hat{U} \sim \sqrt{D^2\left(x^2 - x^{*2}\right)} \qquad \text{for} \quad Dx = O(1) \quad \text{(cf. [1])}, \tag{3.11}$$

$$D \gg 1: \quad \hat{U} \sim D\bar{u}_s(x)\left(1 - 3F_t'(\eta)/[2D\bar{u}_s(x)]^2\right) \quad \text{for} \quad x, \eta = O(1) \quad \text{(cf. [9])}. \tag{3.12}$$

In the first one assumes that $s = O(\tau)$ but the B–V singularity is not taken into account, which points to the situation addressed in issue (ii), Section 1, the second provides the match with the existing theory when evaluated for sufficiently low values of d, unsatisfactory from the viewpoint (i), Section 1. Here both these shortcomings are surmounted by taking D as of $O(1)$ and fix its value by having the canonical representation (3.8), (3.10) of the BL flow terminating at the most downstream position, given by that of the B–V singularity: $x^* = -1$, $\bar{u}_s^* = \bar{u}_d$. This maximum retardation of the breakdown is due to the regularisation of both singularities on basis of the full Reynolds equations that is required to take place at a single streamwise scale much shorter than d. As a result, the following separation criterion relevant for $\sigma/d = O(1)$ gains awareness:

$$D = D^* := [8F_t'(0)/3]^{1/2}, \quad d \sim \left(2^{11/4} f^{1/4} F_t'(0)^{1/2}/3\right) \epsilon^{1/2}/(-\ln \epsilon)^{1/4} \tag{3.13}$$

by (3.6). In the presently proposed theory this criterion replaces that given in [1].

The numerical solution of (3.4) in [17] gives $F_t'(0) \doteq 13.868$ (sensitive to the values of the model input parameters, in particular that of the von Kármán constant, $\kappa \approx 0.384$). Hence, $D^* \doteq 6.081$ and $\bar{u}_{sD}(-1) = \bar{u}_d D^* \doteq 4.651$ are sorted out by (3.13). In order to distinguish between the limits considered in the forerunner studies and here, it is instructive to plot the flow speed $\bar{u}_{sD}$ imposed on the BL in dependence of D and σ related to the scale τ, representative of the occurrence of a velocity defect of $O(1)$: see Figure 3*(a)*. Most important, the canonical flow around the unit cylinder yields $f = 1/3$ by (3.3) and (2.2). From these numbers and (3.13), the separation angle s_d as a function of *Re* is obtained: see Figure 3*(b)*. We recall that the separation point collapses with the trailing edge, $s_d = \pi$, at $Re = \infty$. A comparison of the theoretical predictions with the not so comprehensive set of measured data available, summarised in the textbook [18], emphasises the still notable distance of the separation point from the trailing edge for not too large (but experimentally and practically feasible) values of the Reynolds number $Re_2 := 2\,Re$ (as usual in experiments, formed with the diameter rather than the radius of the cylinder). This is mostly due to the quite weak decay of d as $Re \to \infty$, but a probably insufficient suppression of three-dimensionality of the nominal flow in experiments is also worth mentioning. For the compilation in Figure 3*(b)*, the data points were extracted from the early pioneering wind-tunnel studies [19–21]. We only considered values of Re_2 so large that the attached BLs were confidently viewed as developed turbulent ones in these studies (*transcritical* regime; $Re_2 \times 10^{-6} \gtrsim 3.5$, 1.5, 1.31 in respectively [19], [20], [21]). The data scatter fairly when individual studies are compared, and due to their scarcity in that regime the trend $\partial s_d/\partial Re > 0$ is not reproduced so far. Apparently, the highest value of Re_2 of about 1.782×10^7, achieved in the study [21]), is still hardly surmountable in experiments.

The transformation of the initially moderately-large- to a large-defect BL with a wake-like velocity profile and finally a state of incipient separation when $x = -1$ is visualised in Figure 4. Smooth cubic splines are used to interpolate the data points obtained by numerical evaluation of (2.5), (3.10), (3.8) for $D = D^*$ and $\bar{u}_s = \bar{u}_d - \omega$, $\bar{u}_s = \bar{u}_d - 5i\omega$ with $i = 0, 1, 2, \ldots$, $\omega := 0.425$.

The criterion (3.13) crucially affects the analysis of $\hat{\Psi}$ in the limit $x \to 0_-$ as it induces the formation of a sublayer. We infer from (3.8), (3.10) and (2.6b), (3.5) the following expansions for

$$S \to 0_+: \quad \hat{\Psi} \sim \hat{\Psi}_0(Y) + 3\sqrt{S}\, F_t'(0)\, \hat{\Psi}_0'(Y) \int_0^Y \frac{\mathrm{d}\nu}{\hat{\Psi}_0'(\nu)^2} + O(S), \quad \hat{\Delta} \sim \hat{\Delta}_0 + O\left(\sqrt{S}\right), \tag{3.14}$$

$$Y \to 0: \quad U(Y) := \hat{\Psi}_0'(Y) \sim \left(3/\kappa^{2/3}\right)\left([F_t'(0)/F_t(1)]\, Y/2\right)^{1/3}\left[1 + o(1)\right]. \tag{3.15}$$

Here, $\hat{\Delta}_0 \doteq 1.477$ is found. For (3.14), (3.15) and the subsequent results cf. Figure 4. A novel one-third-power law given by (3.15) replaces the half-power behaviour $\hat{U} - \hat{U}_s \sim 3a(Y/2\hat{U}_s)^{1/2}$ holding for $Y \to 0$ and $-S = O(1)$, according to (3.8) and (3.5). It characterises the velocity profile

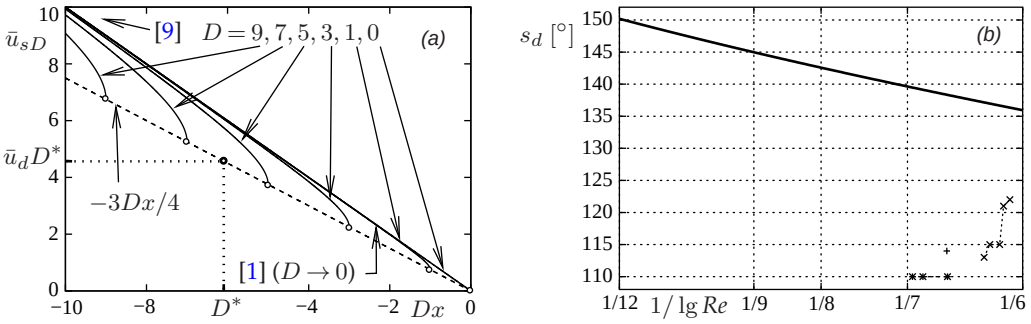

Figure 3. Non-universal counterpart to plot in Figure 2*(a)*, *circles* indicate points of termination *(a)*; predicted separation angles (*solid*) compared to measured ones (+: [19], $Re_2 \times 10^{-6} \approx 8.4$, $s_d \approx 114°$; ×: [20], $2.5 \lessapprox Re_2 \times 10^{-6} \lessapprox 4.0$, $s_d \approx 115°$ for $Re_2 \times 10^{-6} \approx 3.6$; ∗: [21], $Re_2 \times 10^{-6} \approx 8.27, 14.06, 17.82$, $s_d \approx 110°$) *(b)*

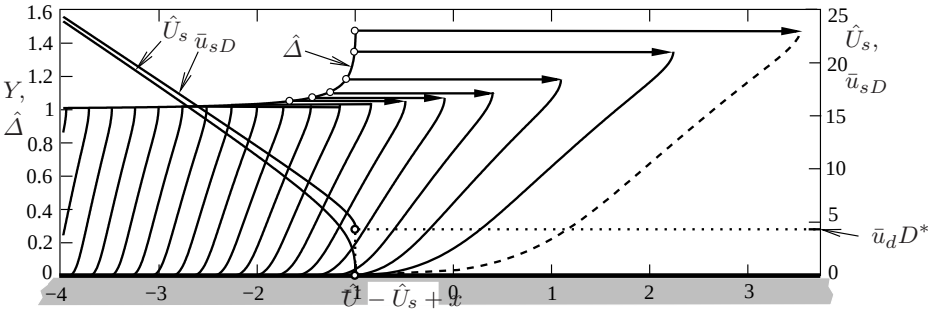

Figure 4. Evolution of BL: *circles* indicate computed data for $\hat{\Delta}$, *dashed* curve represents velocity profile at separation

at separation and the base of the core tier. Its advent is accompanied by a splitting of this layer due to the apparent non-uniformity of the expansion (3.14). It is seen first from (3.8) subject to (3.13) that the B–V singularity is superseded by an even stronger one at the base of the main tier as $\hat{U}_s \sim F_t'(0)^{1/2}(6S)^{1/4}[1 + O(S)]$. Inspection of (2.6b) and (3.5) reveals that the expression for $\hat{U}$ in (3.8) is retained in full if $\zeta := bY/S^{3/4}$ with $b := 4a^2/\left(6^{1/4}D^{*\,3}\right)$, a given in (3.5), is kept fixed. We then have $\hat{\Psi} \sim cSf(\zeta) + \cdots$ with $c := 3D^{*\,4}/(8a^2)$, which, by the specific choice of the constants b and c, yields the problem $f'(\zeta) = (1 + f^{1/2})^{1/2}$, $f(0) = 0$. Integration gives

$$\sqrt{1+\sqrt{f}}\,\left(\sqrt{f}-2\right) = q := \frac{3\zeta}{4} - 2\,, \quad f = (1 + r_+ + r_-)^2\,, \quad r_\pm := \sqrt[3]{\frac{q^2}{2} - 1 \pm q\sqrt{\frac{q^2}{4} - 1}}\,. \tag{3.16}$$

The inversion of the first representation in (3.16) follows by Cardano's method. One finds that $f''(\zeta) > 0$ and $f'''(\zeta) < 0$, cf. Figure 4, and $f \sim q^{4/3} + 2q^{2/3} + O(1)$ as $q \to \infty$. This allows for a direct match of the form of $\hat{\Psi}$ in the sublayer with the two-term expansion (3.14) and confirms the anticipated suppression of terms having the form $\gamma(S)\,\hat{U}(Y)$ in (3.14) with a gauge function γ much larger than $\sqrt{S}$. These describe eigensolutions of the convective operator in the streamwise momentum equation. Here the inviscid nature of the flow prevents their occurrence. Also, (3.16) reveals the transition from the square-root law, yet holding for $q \to 0$, towards the newly found one-third-power law further away from the wall.

The behaviour of the core layer immediately upstream of the B–V singularity differs strikingly from that in [9] (where the singularity is correspondingly weaker), as a consequence of the $O(1)$-velocity deficit ruling here. The emerging inviscid-vortex-flow or Rayleigh problem of self-interacting flow, envisaged next, represents a cornerstone in the current theory of separation. Due to the BL limit and the associated non-linearity and arising surface slip at the base of the core layer

in the oncoming flow, it is not only set apart from that derived in [3] and recovered in [9] but also the central one in [11], which does not allow for a solution confirming consistency of the limit proposed in [1]: cf. item (ii) at the end of Section 1. However, the mechanism elucidated below proves promising as the vorticity originating in the BL upstream enters directly the perturbations considered rather than it forms an inhomogeneity.

4. Local Euler stage

The sudden decrease of the surface slip $\hat{U}_s$ causes the core layer to split into two tiers. Hence, a shortened streamwise length scale comes into play. In the resulting near-wall sublayer, $\hat{\Psi}_Y$ and $\hat{U}_s$ become of comparable magnitude. For a sufficiently severe shortening, the classical hierarchical BL concept is superseded locally by a strong interaction of the BL with the inviscid flow generated on its top, governed by the so induced pressure gradient. Due to the absence of the above eigensolutions, here this typical mechanism is replaced by a radically different one.

(a) Self-interacting inviscid flow

Let us first recall a classical interactive regime, leading to a triple-deck problem. In the main part of the (large-deficit) BL the velocity profile is given by the separating one, here $\lambda\tau U(Y)$, slightly perturbed by the aforementioned eigensolutions, but with γ now superseded by initially unknown displacement functions that vary in streamwise direction, and contributions accounting for a balance of the convective terms with the pressure gradient in the linearised streamwise momentum equation, here about $[u,v]\sim[\lambda\tau U(Y),0]$. Then both the induced pressure and the dominant displacement function are determined by the interaction mechanism, which finally implies a regularisation of a singularity encountered if the classical hierarchical flow description is continued. Interestingly, here this process is stymied as we are left with dominant disturbances of the second type (where the shortened streamwise scale promotes the predominance of the convective over the stress terms). However, the regularisation of the B–V singularity then has to be accomplished by a virtually inviscid flow in the core region itself where the pressure gradient is neither imposed nor, as a consequence, its wall-normal component negligibly small (as it is classically the case). From this the strongest shortening of the scale in s-direction possible ensues, measured by the (local) thickness of the BL, and makes way for a linearised Euler, i.e. a Rayleigh, stage superseding the shear-layer structure. We so arrive at the leading-order approximations

$$\left[\frac{\psi}{\lambda\tau\mu}-\hat{\Psi}_0(Y),\ \frac{p}{(\lambda\tau)^2}\right]\sim\frac{9{D^*}^{3/2}}{16}\sqrt{\frac{\mu}{6\tau}}\,[\Psi,P](X,Y)\,,\quad X:=\frac{s-s_d}{\mu}=\frac{\tau D^*(x+1)}{\mu}\,,\tag{4.1}$$

by virtue of (2.7) and (3.6), and $r_{ij}/(T\tau^2)\sim r^0_{ij}(Y)+\sqrt{\mu/\tau}\,r^1_{ij}(X,Y)$ for $X=O(1)$. Here the "frozen" state of the BL condensed in $[\hat{\Psi},r^0_{ij}](Y)$ is given by its upstream history, whereas $[\Psi,P,r^1_{ij}](X,Y)$ results from solving the accordingly linearised Reynolds equations. This follows by inspection analysis, formally even for $T=O(1)$. The relationships (4.1) and the underlying smallness of the principal perturbation parameter μ/τ, however, again reflect the assumption (3.7): it just delays the emergence of a (then linearised) Euler stage.

(b) Bernoulli sublayer

The sublayer more close to the surface represents the continuation of the corner region where $Y=O(S^{3/4})$, addressed at the end of Section 3(b). Hence, we stipulate that $P(X,Y)$ is bounded for $Y\to0$ and find that $p=O(u^2)$, $r_{ij}=O(Tu^2)$ in this region where $\bar{Y}:=A(\tau/\mu)^{3/4}\,Y=O(1)$ with some constant $A>0$. Then the ratio of $\partial r_{sn}/\partial n$ and $\partial p/\partial s$ is of $O\big(T(\tau/\mu)^{3/4}\big)$ and vanishingly small by (3.7). Consequently, the subregion represents an inviscid shear layer to leading order where Bernoulli's law holds in full. We find that $\psi\sim\lambda(3D^*)^{3/4}/(2^{7/4}A)\,\mu^2\bar{\Psi}(x,\bar{Y})$

as the stretched streamfunction $\bar{\Psi}$ satisfies

$$\bar{U}(x,\bar{\Psi}) := \bar{\Psi}_{\bar{Y}} = \sqrt{2[\bar{B}(\bar{\Psi}) - \bar{P}(X)]}\,, \quad \bar{P}(X) := P(X,0)\,. \tag{4.2}$$

The Bernoulli function $\bar{B}$ is found by matching with the corner region far upstream. To this end, we infer from (4.1) that $X = -SD^{*}\tau/\mu$ and note that $\zeta = (bD^{*\,3/4}/A)\,\bar{Y}/(-X)^{3/4}$. Furthermore, from (2.4) we deduce the dominant varying contribution $-2\bar{u}_d^2\sqrt{S/6}$ to $\bar{p}$ immediately upstream of the B–V singularity, according to (2.6b). From matching $p \sim (\lambda d)^2\bar{p}$ for $S \to 0_+$ and the expression for p in (4.1) for $X \to -\infty$ then follows $\bar{P} \sim -2\sqrt{-X}$ in this limit. When we conveniently choose $A := 3^{3/4}D^{*\,7/4}/(2^{7/4}c)$, matching of ψ results in $\bar{\Psi} \sim -Xf$. Independently, matching of u yields $\bar{B}(\bar{\Psi}) \sim \sqrt{-Xf}$ far upstream for $0 \le f < \infty$. We hence identify $\bar{B}$ with $\sqrt{\bar{\Psi}}$.

The rescaled surface pressure $\bar{P}(X)$ is part of the solution of the Rayleigh problem scrutinised below. It follows that the solution of (4.2), expressed by $\bar{\Psi} = \bar{P}(X)^2 f(\bar{\zeta})$, $\bar{\zeta} := \sqrt{2}\,\bar{Y}/[-\bar{P}(X)]^{3/2}$, and (3.16), exists as long as $\bar{P} \le 0$. We fix a translational invariance of $\bar{\Psi}(X,\bar{Y})$, $\bar{P}(X)$ and hence $\Psi(X,Y)$, $P(X,Y)$ with respect to a shift in X that reflects the accuracy of the leading-order approximations without any loss of generality. Hence, let $X = \bar{Y} = 0$ designate the separation point within the current asymptotic accuracy. We then complete the analysis of the sublayer by noting two results of particular interest. At first, $\bar{U}(X,0) = \sqrt{-2\bar{P}(X)}$ represents the surface slip exerted on the near-wall regions around separation, which are strongly affected by the Reynolds and the viscous shear stresses. Secondly, matching ψ with its two-term expansion in the core region, given by (4.1) as free of eigensolutions proportional to $U(Y)$, verifies (3.15) and yields for

$$Y \to 0: \quad \Psi \sim -[2\kappa^2 F_t(1)/F_t'(0)]^{1/3}\bar{P}(X)\,Y^{2/3}\,. \tag{4.3}$$

This indicates non-uniformity of (4.1) and a new singularity immediately upstream of separation.

(c) The Rayleigh stage — weakening the pressure singularity

In leading order, the momentum equations for the streamwise and wall-normal directions governing the Rayleigh stage in the (locally Cartesian) coordinates X, Y read

$$U(Y)\,\Psi_{YX} - U'(Y)\,\Psi_X = -P_X\,, \quad -U(Y)\,\Psi_{XX} = -P_Y\,. \tag{4.4a,b}$$

By eliminating either Ψ or P, one obtains

$$P_{XX} + P_{YY} = 2(U'/U)(Y)\,P_Y\,, \quad \Psi_{XX} + \Psi_{YY} = (U''/U)(Y)\,\Psi\,. \tag{4.5a,b}$$

In (4.5b), a potentially Y-dependent additive function arising from integration with respect to X is set to zero as a consequence of the conditions of matching with the flow upstream. The inviscid perturbed flow described by (4.4), (4.5) exhibits a vorticity given by the negative right-hand side of (4.5b). By integration of (4.4a), one recovers the linearised Bernoulli's law in the form $P = -U^2(\Psi/U)_Y$. Again, here any additive Y-dependent function is seen to be constant upon differentiation with respect to Y, substitution of P in (4.4b), and by (4.5b). Finally, it turns out to be zero upon insertion of $P \sim \bar{P}$ in the limit $Y \to 0$ into (4.3) and by inspection of (3.15).

The strategy to solve (4.4) does not impose any strong restrictions on $U(Y)$ apart from its generic near-wall behaviour (3.15). We stress that the detailed form $U(Y)$ depends on the turbulence closure used to solve (3.4), which confirms the required continuity of P and P_Y at the local BL edge, $Y = Y_e := \hat{\Delta}_0$. We find that $U_e - U(Y) = O\big((Y_e - Y)^2\big)$ with $U_e := U(\hat{\Delta}_0) = \bar{u}_d D^{*}$ as $Y \to Y_e$, cf. [17], and have to assume that $U(Y) = U_e$ for $Y > Y_e$.

Since the ultimate goal of our effort is the determination of the surface slip $\bar{U}(X,0)$, i.e. $\bar{P}(X)$, we advantageously exploit (4.5a) rather than (4.5b) in the further analysis. As will become evident below, the appearance of P_Y rather than of P on the right-hand side of (4.5a) supports this preference. The boundary conditions are given by the required match with the external flow in the subregion considered in Section 2 and the Bernoulli sublayer. The first owing to (2.4) expressed

through $Z := X + \mathrm{i}Y$ yields for

$$Y > Y_e\,,\quad Z \to \infty: \quad P \sim -2\,\Im\sqrt{Z} = -\sqrt{2\sqrt{X^2+Y^2}-2X}\,. \tag{4.6}$$

The second ensues from (4.3) and by inspection of (4.4b) in the form of a regularity condition for

$$X < 0\,,\quad Y \to 0: \quad P(X,Y) - \bar{P}(X) = O(Y^2)\,. \tag{4.7}$$

Here and in the following the restriction to negative values of X allows for a possible drastic change of the flow structure downstream of separation, accompanied by a breakdown of its current description. More precisely, by the homogeneity of the equations (4.5a,b), their solutions are in general composed by a regular and a irregular contribution. Specifically, the irregular ones to Ψ and P are then associated with the emergence of of eigensolutions in (4.1) and, with the aid of the one-third-power law (3.15), found to be of, respectively, $O(Y^{1/3})$ and $O(Y^{5/3})$ as $Y \to 0$; their suppression gives (4.7). Since (4.6) must provide a match with the behaviour of P as $|X| \to \infty$ for $Y = O(1)$ (via that of P near $Y = Y_e$), (4.5a) with (4.7) yields for

$$X \to -\infty: \quad \frac{P}{(-X)^{1/2}} \sim -2 + g(-X) + \frac{1}{2X^2}\int_0^Y U(\nu)^2\,\mathrm{d}\nu \int_0^\nu \frac{\mathrm{d}\rho}{U(\rho)^2} + o\big(X^{-2}\big)\,. \tag{4.8}$$

The gauge function g with $1 \gg g(X) \gg X^{-2}$ as $X \to -\infty$ is introduced to account for higher-order perturbations in (4.6) and remains undetermined at this stage. The upstream behaviour (4.8) includes the aforementioned one of $\bar{P}(X)$. For $Y \to \infty$, (4.8) indeed complies with (4.6) for any rate of decay of U'/U as $Y_e - Y \to 0_+$. On condition that (4.7) holds even for (sufficiently large) positive values of X, the downstream counterpart to (4.8) starts with some small X-dependent gauge function, predicting the expected decay of P as $X \to \infty$. However, this obviously raises a mismatch with the corresponding behaviour derived from (4.6). This can only be absorbed if the aforementioned change of the flow structure is indeed anticipated by relaxing (4.7) sharply, i.e. disrupting it at a singular point which must coincide with the separation point. We then complement (4.7) to Wiener–Hopf-type boundary conditions, typical for problems describing flow separation in an inviscid limit. Hence, the irregular contribution to P supersedes the regular one at $X = 0$ as we achieve for

$$X > 0\,,\quad Y \to 0: \quad P \to 0\,. \tag{4.9}$$

We then have $\bar{P} = 0$ for $X > 0$, and the new separation singularity is associated with a singular behaviour of P for $Z \to 0$. Finally, we find for

$$X \to \infty: \quad P \sim -\frac{1}{X^{1/2}}\int_0^Y U_r(\nu)^2\,\mathrm{d}\nu + o\big(X^{-1/2}\big)\,,\quad U_r(Y) := \frac{U(Y)}{U_e}\,. \tag{4.10}$$

It is noted that (4.5a) prevents $P(X,Y)$ and its derivatives from assuming local extrema. Thus the relationships $\bar{P} \le 0$, $\bar{P}'(X) \ge 0$ and (4.6), the last giving $P_X > 0$ as $Z \to \infty$, imply $P \le 0$ and $P_X \ge 0$ for $Y \ge 0$.

Let us state the findings (4.7) and (4.9) more precisely as we obtain for

$$Y \to 0: \quad P \sim \bar{P}(X) - 3\bar{P}''(X)\,Y^2/2 + o(Y^2) \quad (X < 0)\,, \quad P = O\big(Y^{5/3}\big) \quad (X > 0)\,. \tag{4.11a,b}$$

On the other hand, P admits a Maclaurin expansion as $X \to 0$ for $Y > 0$ due to the dominance of the X-derivatives in (4.5a). However, the rather abrupt change from a regular to an irregular behaviour of P as $Y \to 0$ is accomplished in a smooth manner in a subregion formed by the half-circle $0 \le \vartheta \le \pi$ with $\vartheta := \arg Z$ in the limit $|Z| \to 0$. There that regular expansion breaks down as all terms in (4.5a) are retained in leading order. One then finds by matching that P admits a purely algebraic behaviour as $|Z| \to 0$. Specifically, we have $P \sim |Z|^\beta G_\beta(\vartheta)$ with some constant $\beta > 0$ and G_β satisfying $G_\beta'' - (2\cot\vartheta/3)\,G_\beta' + \beta(\beta - 2/3)\,G_\beta = 0$. Setting $G_\beta(\vartheta) = (\sin\vartheta)^{5/6}L_l(t)$, $t := \cos\vartheta$

yields the general Legendre equation for the index $5/6$,

$$\left[(1-t^2)L_l'\right]' + \left[l(l+1) - m^2/(1-t^2)\right] L_l = 0\,, \quad l := \beta - 5/6\,, \quad m := 5/6\,. \tag{4.12}$$

Its general solution consists of the linear combination $c_{\rm P}\mathrm{P}_l^{5/6}(t) + c_{\rm Q}\mathrm{Q}_l^{5/6}(t)$ of the associated Legendre functions on the cut (Ferrers' functions) $\mathrm{P}_l^{5/6}(t)$, $\mathrm{Q}_l^{5/6}(t)$. The constants $c_{\rm P}$, $c_{\rm Q}$ and the degree l are determined by the expansion (4.11a), which also ceases to be valid in the circular subregion, and (4.11b) expressed in $|Z|$ and t. To this end, we consider the expansions $L_l \sim a_\mp + b_\mp(1 \pm t)^{5/6} + O(1 \pm t)$ as $t \to \mp 1_\pm$; for the four (l-dependent) coefficients that constitute $a_\mp$, $b_l\mp$ by respective linear combinations we refer to [22]. Matching the representation of P in the circular region and (4.11a) ($t \to -1_+$), (4.11b) ($t \to 1_-$) indicates that

$$a_- := \frac{2^{5/6}\pi}{\Gamma(\frac{1}{6})}\Big(\frac{2\,c_{\rm P}}{\Gamma(\frac{5}{6}-\beta)\Gamma(\frac{1}{6}+\beta)} + \cos\big[(\tfrac{1}{6}+\beta)\pi\big]\,c_{\rm Q}\Big) \tag{4.13}$$

must not vanish ($L_l(-1) \neq 0$) whereas

$$b_- := -\frac{2\pi\,c_{\rm P} + \pi^2\cot(\beta\pi)\,c_{\rm Q}}{\Gamma(\frac{11}{6})\Gamma(-\beta)\Gamma(\beta-\frac{2}{3})}\,, \quad a_+ := \frac{2\,c_{\rm P} - \sqrt{3}\,\pi\,c_{\rm Q}}{2^{1/6}\,\Gamma(\frac{1}{6})} \tag{4.14}$$

must both vanish. The last requirement is equivalent to solving the eigenvalue problem for the eigenvalue l formed by (4.12) subject to $L_l'(-1) = L_l(+1) = 0$. By (4.14), a non-trivial dupel $c_{\rm P}$, $c_{\rm Q}$ is only possible if $\cot(\beta\pi) = -\sqrt{3}$. This yields the discrete set $l = 0, 1, 2, \ldots$, where the non-degenerate case is given by $l = 0$, i.e. $\beta = 5/6$. Then (4.12) can be integrated in closed form to give the linearly independent solutions $\mathrm{P}_0^{-m}(t)$, $\mathrm{P}_0^{-m}(-t)$ [22]. This provides the eigensolution $\mathrm{P}_0^{-5/6}(t) = [(1-t)/(1+t)]^{5/12}/\Gamma(\frac{11}{6})$ and, finally, $G_{5/6}(\vartheta)/G_{5/6}(\pi) = [(1-\cos\vartheta)/2]^{5/6}$. From (4.13), we detect a pressure singularity near separation considerably weaker than the original B–V singularity as we have for

$$X \to 0_-: \quad \bar{P} \sim a_-(-X)^{5/6}\,, \quad a_- = -2^{5/6}\pi\,c_{\rm Q}/\Gamma(\tfrac{1}{6})\,, \quad c_{\rm Q} > 0\,. \tag{4.15}$$

It is noted that in the above Maclaurin expansion the two leading Y-dependent coefficients are unknown, reflecting the ellipticity of (4.5a,b). However, the above local analysis ascribed the two arising coefficients $c_{\rm P}$, $c_{\rm Q}$ to the remaining latter unknown one.

In Figure 5*(a)* the azimuthal variation of P in the circular subregion is plotted. The resultant final splitting of the flow considered in the present study is illustrated in Figure 5*(b)*.

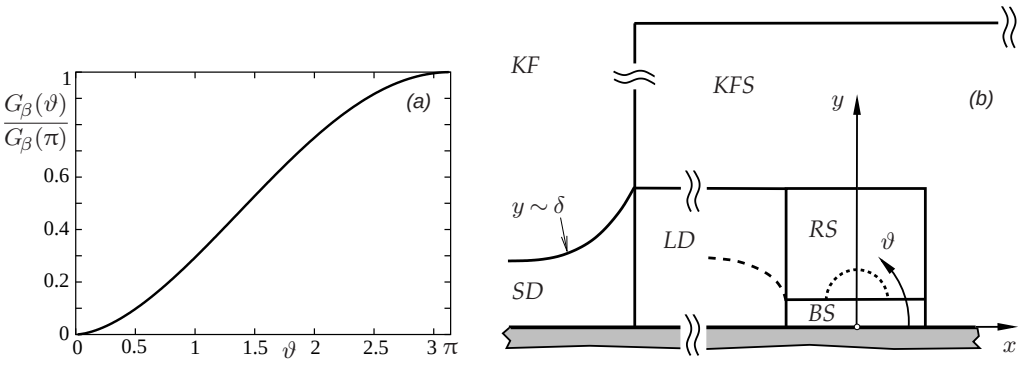

Figure 5. Variation of P around the separation point, $\beta = 5/6$ *(a)*; sketched asymptotic structure of the flow: Kirchhoff flow region *KF*, Kirchhoff flow subregion *KFS*, incident small-defect BL *SD*, large-defect BL *LD*, Rayleigh stage *RS*, Bernoulli sublayer *BS*, *dashed* curves separate subregions arising from non-uniform coordinate expansions *(b)*

(d) On solving the Rayleigh problem

We close the investigations by considering the semi-analytical/numerical strategy we adopt (in a subsequent study) to solve the Rayleigh problem posed by (4.5a), (4.6), (4.7), (4.9), $P(0,0)=0$, and continuity of P and P_Y near $Y=Y_e$. Here the main difficulty arises from the largely unspecified form of $U(Y)$. Denotes $\varkappa$ a wavenumber and $\mathcal{P}(\varkappa)$ the generalised Fourier transform of $\bar{P}'(X)$ – the singularity given by (4.15) is sufficiently weak – with respect to X, the corresponding transform of P_X is expressed as $\mathcal{P}(\varkappa)\,\mathcal{S}(\varkappa,Y)$; we remark that $\mathcal{P}=O\big(|\varkappa|^{-1/2}\big)$ as $\varkappa\to 0$ by (4.8). We then obtain from (4.5a) for

$$0\le|\varkappa|<\infty:\quad(\partial_{YY}-\varkappa^2)\,\mathcal{S}=2(U'/U)(Y)\,\mathcal{S}_Y\,,\quad\mathcal{S}(\varkappa,0)=1\,,\quad(\mathcal{S}_Y/\mathcal{S})(\varkappa,Y_e)=-|\varkappa|\,.\tag{4.16}$$

Here, the last condition suppresses the exponential growth of $\mathcal{S}$ for $Y>Y_e$ and agrees with (4.6). We obtain $\mathcal{S}(\varkappa,Y)=\mathcal{S}(\varkappa,Y_e)\exp(-|\varkappa|\,Y)$ for $Y\ge Y_e$ and find for

$$|\varkappa|\to 0:\quad\mathcal{S}\sim 1-|\varkappa|\int_0^Y U_r(\nu)^2\,\mathrm{d}\nu\left[1-|\varkappa|\left(\int_0^{Ye}U_r(\rho)^2\,\mathrm{d}\rho-\int_\nu^{Y_e}\frac{\mathrm{d}\rho}{U_r(\rho)^2}\right)\right]+O\big(|\varkappa|^3\big)\,,\tag{4.17}$$

with U_r introduced in (4.10). Hence, $\mathcal{S}(\varkappa,Y_e)$ is smooth for $0\le|\varkappa|<\infty$ and $\mathcal{S}(\varkappa,Y)$ for $0\le|\varkappa|<\infty$ and $0<Y<Y_e$. Due to the inhomogeneous boundary condition, the two-point boundary value problem (4.16) then has a solution symmetric in $\varkappa$ and real and unique for all except a set of discrete values of $\varkappa$ where the corresponding (self-adjoint) homogeneous problem has a non-trivial solution. This is solely given by its fundamental solution forming the irregular contribution to P. Also, $\mathcal{S}$ must exhibit a basically exponential tail in the wavenumber space. Specifically, (4.16) suggests the expansion $\mathcal{S}\sim\check{\gamma}(|\varkappa|)\exp(-\check{Y})\,U(Y)[1+O(1/|\varkappa|)]$ for both $|\varkappa|$ and $\check{Y}:=|\varkappa|\,Y$ large and a yet unknown gauge function $\check{\gamma}$ of sub-exponential variation. A near-wall region of non-uniformity arises for $\check{Y}=O(1)$ where we have $\mathcal{S}\sim\check{\mathcal{S}}(\check{Y})$ with $\check{\mathcal{S}}(\check{Y})$ satisfying $\check{\mathcal{S}}''-(2/3)\,\check{\mathcal{S}}'/\check{Y}-\check{\mathcal{S}}=0$, owing to (3.15) and subject to $\check{\mathcal{S}}(0)=1$ and exponential decay rather than growth of $\check{\mathcal{S}}$ for $\check{Y}\to\infty$. The solution $\check{\mathcal{S}}(\check{Y})=2^{1/6}\check{Y}^{5/6}K_{5/6}(\check{Y})/\Gamma(5/6)$ with $K_{5/6}$ specifying a modified Bessel function of the second kind gives $\check{\mathcal{S}}\sim\sqrt{\pi}/\Gamma(5/6)\,(\check{Y}/2)^{1/3}\exp(-\check{Y})[1+O(1/\check{Y})]$ as $\check{Y}\to\infty$, matching the above representation for $\mathcal{S}$. This yields $\check{\gamma}=O(|\varkappa|^{1/3})$, leaving the decay of $\mathcal{S}$ dominated by $\exp(-\check{Y})$ which makes (4.16) amenable to its efficient numerical solution via the discrete cosine transform.

The apparent impossibility to represent $\mathcal{S}$ solely by the regular fundamental solution of the transformed equation (4.5a) confirms the splitting of the near-wall conditions into (4.7) and (4.9). The crucial step then is the determination of $\mathcal{P}$. By (4.7) and (4.9), its real and imaginary part form a Hilbert pair. The same holds for the regular (and the irregular) fundamental solution, which results in two further equations for these parts. This procedure proves self-consistency of the theory within the order of approximation considered.

A further promising aspect supporting existence of the solution is provided by the well-established theory of Beltrami equations. It is sensible to straightly consider the equation $P_{XX}+P_{YY}=(2/C)(C_XP_X+C_YP_Y)$, which reduces to (4.5a) when the function $C(X,Y)$, taken as given, is specified by $U(Y)$. It can be rewritten as $(P_X/C^2)_X+(P_Y/C^2)_Y=0$. (As an appealing interpretation, this expresses the continuity of a potential flow with Cartesian velocity components P_X, P_Y and a density distribution C^{-2}.) Hence, it is equivalent to a system of Beltrami equations: $[P_X,P_Y]=C^2\,[V_Y,-V_X]$; specifically, here (4.4) yields $V(X,Y)=-\Psi_X/U$. These are known to be invariant against a conformal mapping, $X+\mathrm{i}Y\mapsto\xi+\mathrm{i}\upsilon$, say, such that $[\Pi,\Upsilon](\xi,\upsilon):=[P,V](X,Y)$ and $\Gamma(\xi,\upsilon):=C(X,Y)$ satisfy $[\Pi_\xi,\Pi_\upsilon]=\Gamma^2\,[\Upsilon_\upsilon,-\Upsilon_\xi]$. Accordingly, the original equation is transformed into $\Pi_{\xi\xi}+\Pi_{\upsilon\upsilon}=(2/\Gamma)(\Gamma_\xi\Pi_\xi+\Gamma_\upsilon\Pi_\upsilon)$. The idea here is to construct the above conformal mapping such that Γ is given in the simplest form conceivable.

5. Conclusions and further outlook

A rigorous theory on turbulent bluff-body separation under the premise that the turbulence intensity attains the highest level possible in the limit of large Reynolds numbers Re

was presented. One intriguing finding is the necessity of a large velocity deficit in the boundary layer flow on a small streamwise length scale that measures the distance d of the position of the Brillouin–Villat singularity from the trailing edge which emerges in the limit of a fully attached potential flow, seen as a limiting state of Kirchhoff flows. It was shown the first time how this BL evolves in (an universal manner) from an initially firmly attached turbulent BL having a small velocity deficit towards one on the brink of separation. There the velocity profile admits a novel one-third power variation with distance from the wall. Insofar as a generic separation criterion was formulated by virtue of the distinguished limit $d \to 0$ as $Re \to \infty$ considered, the present theory represents the "missing link" bridging the gap between the cases addressed in (i) and (ii) at the end of Section 1. The (preliminary) analysis of the Rayleigh problem finally ensuing from the breakdown of the shear layer limit raises hope that its solution allows for completing the theory to a fully self-consistent flow description.

Open points of massive interest currently under investigation include the numerical solution of the Rayleigh problem by a spectral method, in particular the distributions of the surface pressure and the associated slip velocity that drives the multi-structured near-wall flow. Disregarded in the present approach, the latter is crucially affected by the shear stresses which bring that slip to rest. Therefore, it is first of paramount interest how the new pressure singularity encountered in the Rayleigh stage close to separation and the associated transition of the surface pressure are modified by the Bernoulli sublayer. Subsequent efforts will aim at disclosing how the so altered singularity emerging at the base of the region where an Euler flow prevails and more close to the separation point affects that near-wall flow. As the regularisation of this singularity can only be accomplished beyond the inviscid limit considered here, the near-wall flow must abandon its hitherto passive role locally. Eventually, we expect to detect a novel mechanism of viscous-inviscid flow interaction as the classical triple-deck structure is suppressed by the extreme retardation of separation. The question arises whether, unlike in the forerunner study [9], here the logarithmic law of the wall is eradicated when the wall shear stress changes sign at the effective position of separation. A most comprehensive understanding of the near-wall flow will then refine the separation criterion and hence complete the local picture of gross separation.

Further issues concern the full Euler stage replacing the Rayleigh stage once the present constraint on the turbulence intensity level is relaxed to allow for a fully developed turbulent flow. Regarding the flow on the body scale and beyond, the current theory predicts zero body drag in the limit $Re \to \infty$, but this may be in doubt if a further transition of the separated shear layers towards massive fully developed turbulent ones has taken place. First ideas are reported in the survey paper [23]; for more recent developments we refer to the consecutive papers [24,25]. Finally, the validation of the theory by comparison with measurements deserves intensified attention. For the time being, this can be seen as promising in the light of the surprising scarcity of publicly available data for a most two-dimensional averaged flow around a circular cylinder.

Acknowledgements. This research was partially funded by the Austrian Research Promotion Agency (FFG) within the Austrian Competence Centers for Excellent Technologies (COMET) K2 Programme (FFG grant no.: 824187, project acronym: *XTribology*).

References

1. Neish A, Smith FT. 1992 On turbulent separation in the flow past a bluff body. *J. Fluid Mech.* **241**, 443–467. (doi:10.1017/S0022112092002118)
2. Sychev VV, Ruban AI, Sychev Vic.V, Korolev GL. 1998 *Asymptotic Theory of Separated Flows*, eds. Messiter AF, Van Dyke MD. Cambridge, UK: Cambridge University Press.
3. Melnik RE, Chow R. 1975 Asymptotic Theory of Two-Dimensional Trailing-Edge Flows. In *Aerodynamic Analyses Requiring Advanced Computers*. Part II. NASA SP–347, pp. 177–249. Washington, DC: NASA.
4. Sychev VV, Sychev Vik.V. 1980 On turbulent separation. *U.S.S.R. Comput. Math. Math. Phys.* **20**, 133–145.
5. Sychev Vik.V. 1983 Asymptotic theory of turbulent separation. *Fluid Dyn.* **18**(4), 532–538.

(doi:10.1007/BF01090616)
6. Sychev Vik.V. 1987 Theory of self-induced separation of a turbulent boundary layer. *Fluid Dyn.* **3**(22), 371–379. (doi:10.1007/BF01051916)
7. Melnik RE. 1989 An asymptotic theory of turbulent separation. *Comput. Fluids* **17**(1), 165–184. (doi:10.1016/0045-7930(89)90014-5)
8. Stewartson K. 1970 Is the singularity at separation removeable? *J. Fluid Mech.* **44**(2), 347–364. (doi:10.1017/S0022112070001866)
9. Scheichl B, Kluwick A, Smith FT. 2011 Break-away separation for high turbulence intensity and large Reynolds number. *J. Fluid Mech.* **670**, 260–300. (doi:10.1017/S0022112010005306)
10. Scheichl B, Kluwick A, Alletto M. 2008 "How turbulent" is the boundary layer separating from a bluff body for arbitrarily large Reynolds numbers? *Acta Mech.* **201**(1–4), 131–151 (invited). (doi:10.1007/s00707-008-0078-7)
11. Scheichl B, Kluwick A. 2008 Asymptotic theory of bluff-body separation: a novel shear-layer scaling deduced from an investigation of the unsteady motion. *J. Fluids Struct.* **24**(8), 1326–1338. (doi:10.1016/j.jfluidstructs.2008.07.001)
12. Vanden-Broeck J-M. 2010 *Gravity–Capillary Free-Surface Flows*. Oxford, UK: Oxford University Press.
13. Scheichl B, Kluwick A. 2008 Level of Turbulence Intensity Associated with Bluff-Body Separation for Large Values of the Reynolds Number. AIAA Meeting Paper 2008-4348. (doi:10.2514/6.2008-4348)
14. Gurevich MI. 1966 *The Theory of Jets in an Ideal Fluid*. International Series of Monographs in Pure and Applied Mathematics, vol. 93. Oxford, UK: Pergamon Press.
15. Kolscher M. 1940 Unstetige Strömungen mit endlichem Totwasser. *Luftfahrtforsch.*, **17**(5), 154–160 (in German).
16. Kraemer K. 1963 Die Potentialströmung mit Totwasser an einer geknickten Wand. *Arch. Appl. Mech. (Ing.-Arch.)* **33**(1), 36–50 (in German). (doi:10.1007/BF00537618)
17. Scheichl B., Kluwick A. 2013 Non-unique turbulent boundary layer flows having a moderately large velocity defect: a rational extension of the classical asymptotic theory. *Theor. Comput. Fluid Dyn.* **27**(6), 735–766. (doi:10.1007/s00162-012-0266-x)
18. Zdravkovich MM. 1997 *Flow Around Circular Cylinders. A Comprehensive Guide Through Flow Phenomena, Experiments, Applications, Mathematical Models, and Computer Simulations. Vol. 1: Fundamentals*, chap. 6–7. Oxford (UK), New York, Tokyo: Oxford University Press.
19. Roshko A. 1961 Experiments on the flow past a circular cylinder at very high Reynolds number. *J. Fluid Mech.* **10**(3), 345–356. (doi:10.1017/S0022112061000950)
20. Achenbach E. 1968 Distribution of local pressure and skin friction around a circular cylinder in cross-flow up to $Re = 5 \times 10^6$. *J. Fluid Mech.* **34**(4), 625–639. (doi:10.1017/S0022112068002120)
21. Jones GW, Cincotta JJ, Walker RW. 1969 Aerodynamic Forces on a Stationary and Oscillating Circular Cylinder at High Reynolds Numbers. NASA TR R-300 (Document ID: 19690007972). Washington, DC: NASA.
22. Olver FOW, Lozier DW, Boisvert RF, Clark CW. (eds.) 2010 *NIST Handbook of Mathematical Functions*. National Institute of Standard and Technologies (US Department of Commerce). Cambridge (UK), New York: Cambridge University Press. See http://dlmf.nist.gov/.
23. Smith FT, Scheichl B, Kluwick A. 2010 On turbulent separation (James Lighthill Memorial Paper 2010). *J. Eng. Math.* **68**(3–4), 373–400. (doi:10.1007/s10665-010-9413-9)
24. Sychev Vic.V. 2010 On asymptotic theory of separated flows past bodies. *Fluid Dyn.* **45**(3), 441–457. (doi:10.1134/S0015462810030117)
25. Sychev Vic.V. 2011 On regions of turbulence in separated flows. *TsAGI Science Journal* **42**(5), 555–563. (doi:10.1615/TsAGISciJ.2011004313)